SEA STATE MONITORING BY SHIP MOTION MEASUREMENT AND ANALYSIS TO INCREASE THE SAFETY OF SHIPS AND NAVIGATION

SILVIA ASCIONE

SILVIAASCIONE

SEA STATE MONITORING BY SHIP MOTION MEASUREMENT AND ANALYSIS TO INCREASE THE SAFETY OF SHIPS AND NAVIGATION

UNIVERSITY OF NAPLES PARTHENOPE
DEPARTMENT OF SCIENCE AND TECHNOLOGY
PhD Thesis

PhD in Environmental Phenomena and Risks
XXXVIII Cycle

UNIVERSITY OF NAPLES PARTHENOPE

DEPARTMENT OF SCIENCE AND TECHNOLOGY

PhD in Environmental Phenomena and Risks

XXXVIII Cycle

Sea State Monitoring by Ship Motion Measurement and Analysis to Increase the Safety of Ships and Navigation

SSD: IIND-01/B - Ship Structures and Engineering

Tutor:
Prof. Vincenzo Piscopo

PhD Candidate:
Silvia Ascione

Doctorate Coordinator:
Prof. Antonio Occhiuzzi

Academic Year 2024/2025

This page is intentionally left blank.

Abstract

Knowledge of sea state conditions is of central importance for a wide range of maritime operations. This thesis presents two novel numerical methods for estimating unimodal and bimodal short-crested seas. Both methods are formulated in the frequency domain as parametric models and employ the JONSWAP spectrum to parameterise the wave spectra. The developed numerical procedures are validated through extensive tests, using synthetic ship motion data, generated by a MATLAB code, specifically developed for this research. Additionally, the unimodal method is further validated using a set of full-scale data. The results demonstrate promising performances and confirm the accuracy of the proposed estimation techniques. Overall, this study demonstrates that these numerical approaches can significantly enhance the ship safety and contribute to the environmental protection if appropriately integrated with the on-board decision-making systems.

Riassunto

La conoscenza dello stato del mare è di fondamentale importanza per un'ampia gamma di operazioni marittime. In questa tesi vengono presentati due nuovi metodi numerici per stimare mari a cresta corta unimodali e bimodali. Entrambi i metodi sono formulati nel dominio della frequenza come modelli parametrici, e utilizzano lo spettro JONSWAP per descrivere le caratteristiche degli spettri d'onda. Le procedure numeriche sono state validate attraverso test approfonditi, utilizzando dati simulati dei moti nave, opportunamente generati con un codice MATLAB sviluppato per questa ricerca. Per il metodo unimodale, è stata condotta una validazione aggiuntiva utilizzando dati reali. I risultati ottenuti evidenziano prestazioni promettenti e confermano l'accuratezza delle tecniche proposte. Nel complesso, questo studio dimostra come tali approcci numerici possano contribuire in maniera significativa alla sicurezza delle navi e alla tutela dell'ambiente, se integrati in modo appropriato nei sistemi decisionali a bordo.

Preface

This thesis is submitted in partial fulfilment of the requirements for the PhD degree. The PhD studies have been carried out at the University of Naples Parthenope, at the Department of Science and Technology, under the supervision of Associate Professor Vincenzo Piscopo. The research took place from November 2022 to October 2025.

During my PhD studies, I spent six months abroad at the Technical University of Denmark (DTU), at the Department of Civil and Mechanical Engineering, Section of Fluid Mechanics, Coastal and Maritime Engineering, under the supervision of Associate Professor Ulrik Dam Nielsen.

The PhD studies were financially supported by the European Union–NextGenerationEU, National Recovery and Resilience Plan (PNRR), Missione 4 Componente 2 Investimento 1.4 'Potenziamento strutture di ricerca e creazione di campioni nazionali di R&S su alcune Key Enabling Technologies'. Code CN00000023 – Title: Sustainable Mobility Center (Centro Nazionale per la Mobilità Sostenibile)–CNMS.

This page is intentionally left blank.

List of Attended Conferences

1. 2024 IEEE International Workshop on Metrology for the Sea, Learning to Measure Sea Health Parameters, 14-16 October 2024, Portorož, Slovenia.

2. 2023 IEEE International Workshop on Metrology for the Sea, Learning to Measure Sea Health Parameters, 4-6 October 2023, Valletta campus, Malta.

3. 21st International Conference on Numerical Analysis and Applied Mathematics, 11-17 September 2023, Crete, Greece.

Award

1. Best Poster at the 2024 IEEE International Workshop on Metrology for the Sea, Learning to Measure Sea Health Parameters, titled "Comparison of Linear and Rank-Correlation for the Sea State Estimation", authored by Ascione S., Piscopo V. and Scamardella A.

List of publications

This section lists the publications produced during the PhD years. They are subdivided into three categories: conference publications, journal articles and, finally, additional papers that are not part of this thesis.

Conference publications

1. Ascione, S., Nielsen, U. D., Piscopo, V., (2024a). Validation of the Sea State Estimation Method Using a Simulated Ship Motions Dataset. *Proceedings of the 2024 IEEE International Workshop on Metrology for the Sea, Learning to Measure Sea Health Parameters, Portorož, Slovenia, 14-16 October 2024*, 176–180.

2. Ascione, S., Piscopo, V., Scamardella, A., (2024b). Comparison of Linear and Rank-Correlation for the Sea State Estimation. *Proceedings of the 2024 IEEE International Workshop on Metrology for the Sea, Learning to Measure Sea Health Parameters, Portorož, Slovenia, 14-16 October 2024*, 250-255.

3. Ascione, S., Gaglione, S., Piscopo, V., Scamardella, A., (2023). Incidence of parametrized methods for spectral analysis of Ship Motion. *Proceedings of the 2023 IEEE International Workshop on Metrology for the Sea, Learning to Measure Sea Health Parameters, Valletta campus, Malta, 4-6 October 2023*, 170-175.

Journal articles

1. Ascione, S., Nielsen, U.D., Piscopo, V., Storhaug, G, (2026). Sea state reconstruction based on the Spearman rank correlation using full-scale data from a containership. *Ocean Engineering*. 343(123471).

2. Piscopo, V., Ascione, S., Scamardella, A., (2025). Assessment of bimodal sea states by the wave buoy analogy method. *Ocean Engineering*. 340(122258).

3. Piscopo, V., Ascione, S., Scamardella, A., (2024). A new wave spectrum assessment procedure based on Spearman rank correlation algorithm. *Ocean Engineering*. 308(118348).

Other papers published, not part of this thesis.

1. Cappello, G., Angrisano, A., Ascione, S., Del Pizzo, S., Gioia, C., Portelli, G., Susi, M., Gaglione, S., (2023). Demonstrating Galileo Has in Single Point Positioning, *Proceedings of the 2023 IEEE International Workshop on Metrology for Automotive (MetroAutomotive), Modena, Italy, 28-30 June 2023*, 117-121.

2. Angrisano, A., Ascione, S., Cappello, G., Gioia, C., Gaglione, S., (2023). Application of "Galileo High Accuracy Service" on single-point positioning. *Sensors*, 23(9), 4223.

Thesis Outline

The contents of this thesis are organised into eight chapters. Chapter 1 introduces the topic of sea state estimation and provides a brief overview of the wave buoy analogy method. Chapter 2 outlines the theoretical background on ocean waves and introduces the models of wave spectra. Chapter 3 presents the code developed to generate the ship motion dataset in the time domain, based on the employment of the Cummins equations. Chapters 4 and 5 focus on the theoretical issues concerning the state estimation and outline the numerical procedures developed for unimodal and bimodal sea state conditions, respectively. More specifically, Chapter 4 focuses on the method proposed by Piscopo et al. (2024), which addresses sea state estimation under unimodal short-crested conditions. Instead, Chapter 5 introduces the numerical procedure developed by Piscopo et al. (2025) for estimating bimodal sea states, characterised by the simultaneous presence of swell and wind sea wave components. Chapters 6 and 7 present the results of the research on the assessment of sea state parameters. In particular, Chapter 6 is divided into three sections. The first provides details on the reference ship, while the remaining ones report the main findings related to the validation of the unimodal procedure. Precisely, the second section includes the benchmark study and the statistics of errors from Piscopo et al. (2024), together with the results discussed in Ascione et al. (2024), which investigate the incidence of the linear and rank correlation coefficients. Instead, the third section discusses the main outcomes derived from a set of full-scale data (Ascione et al., 2026). Chapter 7 is dedicated to the results of the sea state reconstruction algorithm under bimodal conditions, as reported in Piscopo et al. (2025). Finally, Chapter 8 outlines the conclusions and provides some advice for future research. All papers that are part of this thesis are attached in Appendix A.

Contents

List of Figures

List of Tables

List of Symbols and Acronyms

$\bar{\beta}$	Estimated prevailing wave direction
$\bar{\beta}_s$	Estimated swell prevailing wave direction
$\bar{\beta}_w$	Estimated wind sea prevailing wave direction
$\bar{\beta}_{\bar{n}}$	Optimum directional heading angle conditional on optimum spreading parameter
$\bar{\beta}_{eq}$	Estimated normalized equivalent prevailing wave direction
$\bar{\beta}^*_{eq}$	Estimated equivalent prevailing wave direction
$\bar{\gamma}$	Estimated peak enhancement factor
$\bar{\gamma}_s$	Estimated peak enhancement factor of the swell component
$\bar{\gamma}_w$	Estimated peak enhancement factor of the wind sea component
$\bar{\mu}_{\bar{n}}$	Optimum heading angle of prevailing wave direction conditional on optimum estimated spreading parameter
$\bar{\omega}_s$	Estimated separation frequency
$\bar{H}^{ii}_{s,\bar{n}}$	Significant wave height conditional on i-th motion conditional on optimum spreading parameter
$\bar{H}^{ii}_{s,\tilde{n}}$	Significant wave height conditional on i-th motion conditional on tentative spreading parameter
$\bar{H}_s$	Estimated significant wave height
$\bar{H}_{s,\tilde{n}}$	Significant wave height conditional on tentative spreading parameter
$\bar{H}_{s,eq}$	Estimated equivalent significant wave height
$\bar{H}_{s,s}$	Estimated significant wave height of the swell component

$\bar{H}_{s,w}$	Estimated significant wave height of the wind sea component
$\bar{n}$	Optimum spreading parameter
$\bar{S}_{ij}$	Estimated ship acceleration spectrum of the i, j-th motion
$\bar{T}_p$	Estimated wave peak period
$\bar{T}_{e,eq}$	Estimated equivalent wave energy period
$\bar{T}_{e,s}$	Estimated swell wave energy period
$\bar{T}_{e,w}$	Estimated wind sea wave energy period
$\bar{T}_{p,\bar{n}}$	Optimum wave peak period conditional on optimum spreading parameter
$\bar{T}_{p,eq}$	Estimated equivalent wave peak period
$\bar{T}_{p,s}$	Estimated swell wave peak period
$\bar{T}_{p,w}$	Estimated wind sea wave peak period
β_s	Prevailing wave direction of swell component
β_w	Prevailing wave direction of wind sea component
$\ddot{\xi}_i$	Acceleration of the i-th motion mode
Δ	Ship displacement
δ	Heading angle of the elementary wave train as regards the ship reference frame
$\Delta\omega_e$	Wave frequency interval
$\dot{\xi}_i$	Velocity of the i-th motion mode
ϵ_i	Phase angle of the i-th motion mode
η	Wave Amplitude
Γ	Gamma function
γ	Spectral width parameter
$\gamma_{\max}$	Upper bound value of peak enhancement factor interval
γ_s	Peak enhancement factor of the swell spectrum
γ_w	Peak enhancement factor of the wind sea spectrum

$\hat{\sigma}$	Spectral width parameter conditioned by the peak circular frequency
$\hat{S}$	Hermitian cross-spectral matrix of measured ship motions
λ	Wavelength
S	Matrix of ship acceleration spectra
μ	Heading angle of the elementary wave train as regards the ship reference frame
μ_n	Wave propagation
ω	Absolute wave circular frequency
ω_e	Encounter wave circular frequency
ω_n	Angular frequency
ω_p	Wave peak frequency
$\overline{\eta}$	Mean sea surface level
ϕ	Random phase shift
Φ_i	Complex wave exciting force function per unit wave amplitude of the i-th motion mode
ψ	Doppler shift function
ρ	Water density
σ	Standard deviation
σ^2	Wave variance
$\tilde{\gamma}$	Tentative peak enhancement factor
$\tilde{\gamma}_{\tilde{n}}$	Tentative peak enhancement factor conditional on tentative spreading parameter
$\tilde{\gamma}_{max}$	Maximum tentative peak enhancement factor
$\tilde{\gamma}_{min}$	Minimum tentative peak enhancement factor
$\tilde{\lambda}$	Shape parameter of the Ochi-Hubble wave spectrum
$\tilde{\mu}_{\tilde{n}}$	Tentative heading angle of prevailing wave direction conditional on tentative spreading parameter
$\tilde{\omega}_s$	Tentative separation frequency

$\tilde{\omega}_{(s,max)}$ Maximum tentative separation frequency

$\tilde{\omega}_{(s,min)}$ Minimum tentative separation frequency

$\tilde{a}_{i,s}$ Swell tentative filtered acceleration of the i-th motion mode

$\tilde{a}_{i,w}$ Wind sea tentative filtered acceleration of the i-th motion mode

$\tilde{c}_S$ Tentative Spearman correlation coefficient after Fisher z-transformation

$\tilde{c}_{ii}$ Correlation coefficient of tentative spectrum for the i-th motion mode

$\tilde{c}_{ij}^{i}$ Tentative Spearman correlation coefficient for the imaginary part of cross spectra

$\tilde{c}_{ij}^{r}$ Tentative Spearman correlation coefficient for the real part of cross spectra

$\tilde{h}_{ij}$ Tentative ship motion acceleration spectrum for unit wave amplitude

$\tilde{n}$ Tentative spreading parameter

$\tilde{S}$ Tentative Hermitian cross-spectral matrix of ship motions

$\tilde{S}_e$ Tentative wave spectrum in the encounter wave frequency domain

$\tilde{S}_s$ Swell tentative filtered matrix of ship acceleration spectra

$\tilde{S}_w$ Wind sea tentative filtered matrix of ship acceleration spectra

$\tilde{S}_{(e,1)}$ Tentative short-crested wave spectrum with unit wave amplitude in the encounter frequency-domain

$\tilde{S}_{(e,1)}^{k}$ Tentative k-th component of the short-crested wave spectrum with unit wave amplitude in the encounter frequency-domain

$\tilde{S}_{ij}$ Tentative ship acceleration spectrum of the i, j-th motion

$\tilde{s}_{ij}$ Tentative spectral function

$\tilde{T}_p$ Tentative wave peak period

$\tilde{T}_{p,\tilde{n}}$ Tentative wave peak period conditional on tentative spreading parameter

$\tilde{T}_{p,max}$ Maximum tentative wave peak period

$\tilde{T}_{p,min}$ Minimum tentative wave peak period

ϑ Heading angle of the elementary wave train as regards the prevailing wave direction

ξ_i Amplitude of the i-th motion mode

A	Added mass vector
a_k	k-th component of the ship acceleration vector
a_n	Amplitude of the n-th wave component
A_{ij}	Added mass corresponding to the i, j-th motion mode
A_{ij}^0	Zero-speed added mass corresponding to the i, j-th motion mode
A_{ij}^∞	Added mass at infinite frequency corresponding to the i, j-th motion mode
B	Hydrodynamic damping vector
B_{ij}	Hydrodynamic damping corresponding to the i, j-th motion mode
B_{ij}^0	Zero-speed hydrodynamic damping corresponding to the i, j-th motion mode
B_{ij}^∞	Hydrodynamic damping at infinite frequency corresponding to the i, j-th motion mode
C_{ij}	Hydrodynamic restoring coefficient corresponding to the i, j-th motion mode
D	Spreading function
d	Water depth
F_i	Random force corresponding to the i-th motion mode
f_i	Exciting wave force per unit wave amplitude corresponding to the i-th motion mode
g	Gravity acceleration
H	Wave height
H_i	Ship transfer function for the i-th motion mode
H_s	Significant wave height
$H_{s,s}$	Significant swell wave height
$H_{s,w}$	Significant wind sea wave height
k_n	Wave number
k_{ij}	Impulse response function of the i, j-th motion mode
m_n	Spectral moment
n	Spreading parameter

$n_{\max}$ Upper bound of spreading parameter interval

$n_{\min}$ Lower bound of spreading parameter interval

n_s Spreading parameter of the swell component

n_w Spreading parameter of the wind sea component

p Percentile

Q_p Quartile at the percentile p

S Long-crested wave spectrum in the absolute frequency-domain

$S(\omega)$ Wave spectrum for long-crested seas

$S(\omega, \mu)$ Directional wave spectrum

S_0 Short-crested wave spectrum in the absolute frequency-domain

$S_\sigma(\omega)$ Wave variance spectrum

S_B Bretschneider spectrum

S_b Bimodal wave spectrum

S_e Short-crested wave spectrum in the encounter frequency-domain

S_J JONSWAP wave spectrum

S_{ij} Ship acceleration spectrum of the i, j-th motion

S_{OH} Ochi-Hubble spectrum

S_{PM} Pierzon Moskowitz spectrum

S_{TMA} TMA spectrum

T_p Wave peak period

$T_{p,\max}$ Upper bound value of wave peak period interval

$T_{p,\min}$ Lower bound value of wave peak period interval

$T_{p,s}$ Wave peak period of the swell component

$T_{p,w}$ Wave peak period of the wind sea component

U Ship speed

V Wind speed

ADOPT Advanced Decision Support System for Ship Design

AE Absolute Error

ANN Artificial Neural Network

BEM Boundary Element Methods

CNNs Convolutional Neural Networks

IMO International Maritime Organization

MAE Mean Absolute Error

MASS Maritime Autonomous Surface Ship

MSC Maritime Safety Committee

ODE Ordinary Differential Equation

PFD Probability Density Function

SWAN Simulating WAve Nearshore

WAM WAve Model

WW3 Wavewatch III

Chapter 1

Introduction

1.1 Background

Over the past 36 years, more than 63,991 maritime accidents (an average of 1,777 per year) have occurred (Luo and Shin, 2019), causing significant loss of life and environmental damage. Indeed, seafaring has been defined as one of the world's most dangerous occupations (Håvold, 2005). In this respect, the International Maritime Organization (IMO) declared that the main causes of these accidents include interconnected factors, such as design faults, human error, inadequate technological equipment and poor maintenance (IMO, 2008). In addition to these factors, adverse environmental conditions, such as the presence of high waves encountered during navigation, can induce dynamic instabilities of the vessel. This risk can be mitigated by installing on-board decision support systems, which assist the master and the crew in making safe decisions in real time. However, the effectiveness of such systems strongly depends on the assessment of sea state parameters. For this reason, sea state estimation has become a widely investigate topic in the maritime research field area. Evidence of the growing interest in this area is shown in Figure 1.1, using the database retrieved from the Scopus library (Elsevier, 2024). The histogram provides an overview of the annual number of publications from 1980 to 2024 containing the keyword "sea state estimation". Furthermore, based on the institutional affiliations of the contributing authors, Figure 1.2 shows the most active countries in this research area. The highlighted nations, namely Denmark, Norway, Italy, Japan, Australia, Brazil, the United Kingdom and China, demonstrate a strong presence in the scientific literature on sea state estimation.

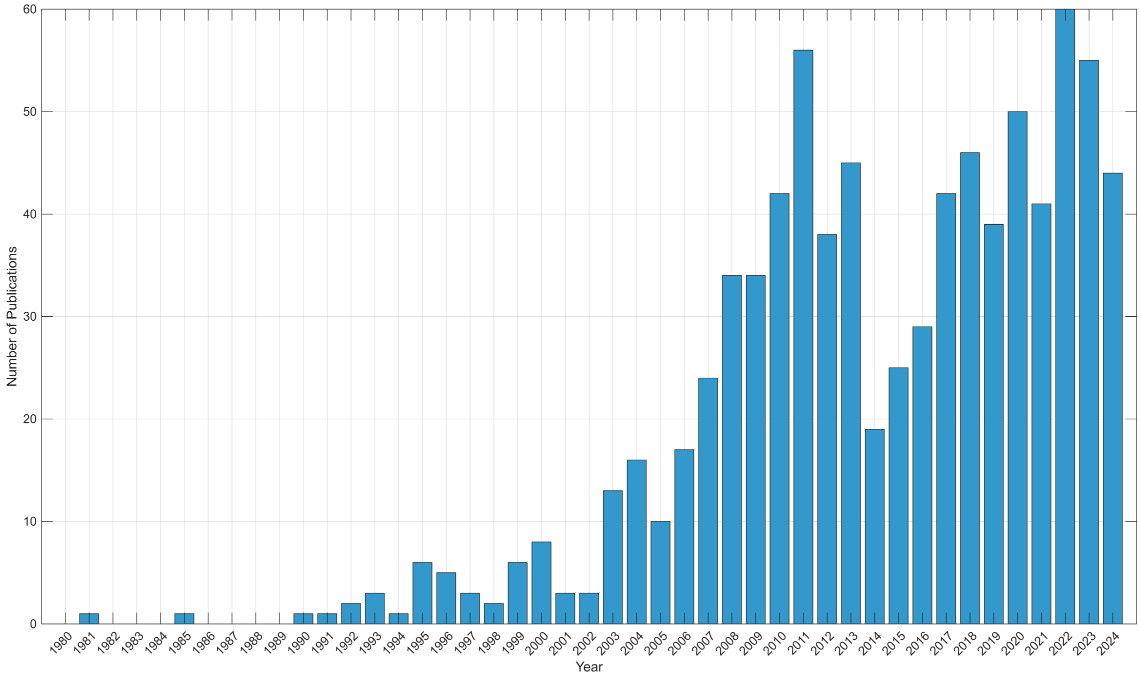

Figure 1.1: Annual number of scientific publications containing the keyword "sea state estimation" (1980–2024), based on data retrieved from the Scopus database (Elsevier, 2024).

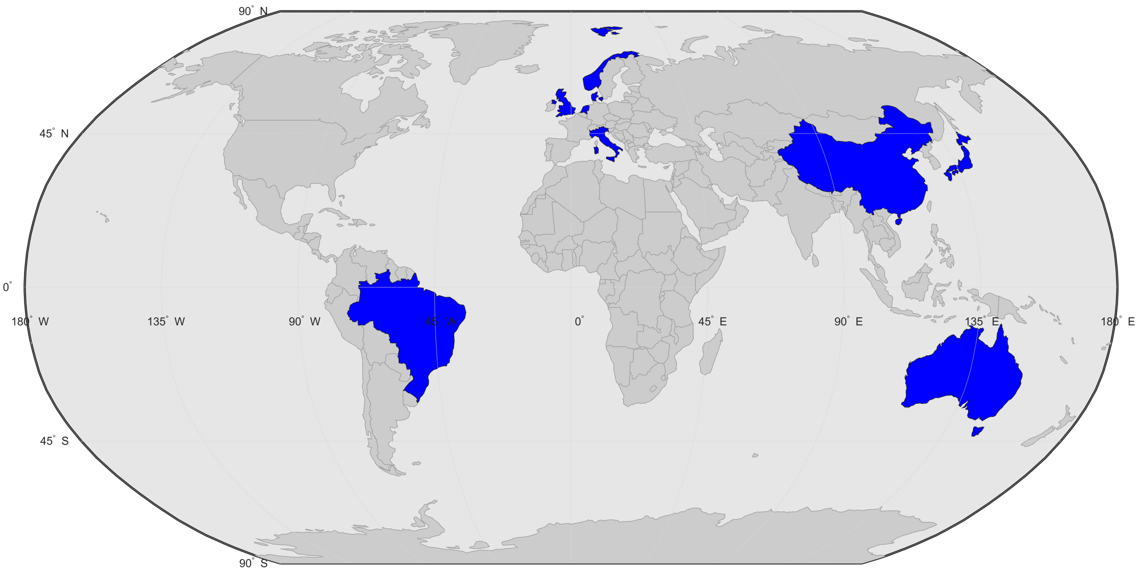

Figure 1.2: Geographical distribution of countries with significant research findings in sea state estimation (Elsevier, 2024).

1.2 Sea State Estimation: an overview

Sea state estimation is a multidisciplinary research topic devoted to measuring the main wave parameters at a specific location and time. The ocean is a complex and dynamic environment, influenced by various interconnected factors such as wind speed and direction, tides, currents and bathymetry (González et al., 2004). In this respect, the reliable assessment of sea state conditions is essential for many applications. In the offshore sector, information about the sea state represents a crucial prerequisite for designing structures, as hydrodynamic wave loads can significantly impact structural integrity (Nestegård et al., 2006, Ergin et al., 2018). For instance, offshore sites in West Africa, Brazil and Southeast Asia are generally subject to more regular sea conditions than the North Sea and the Gulf of Mexico, which are known for rough seas and frequent hurricanes (Chakrabarti, 2005). In the oceanographic field, sea state data are crucial not only for the validation and enhancement of forecasting and nowcasting models, but also for analysing interaction mechanisms and energy fluxes at the ocean–atmosphere interface (Stammer and Chassignet, 2000). In the context of the safety of ships and navigation, beyond avoiding the occurrence of ship instabilities, sea state estimation can be useful to plan the optimal route based on the on-board decision support systems. These systems are currently designed to enhance navigation safety and collision avoidance, assist in risk assessment for decision-making and analyse cybersecurity risks (Mansouri et al., 2015). Another important aspect of planning a safe route is the applicability of weather routing criteria to optimise the ship voyage duration and reduce the fuel consumptions and emissions in the atmosphere. The pioneering studies on weather routing criteria were presented by Zoppoli (1972) and James (1975). In this field, several methods and approaches have been presented in the literature and among them, one of the methods that solves the problem of finding the shortest path from a point in a graph (the source) to a destination is the Dijkstra algorithm (Dijkstra, 1959). The limitation of this algorithm is that it can handle only one objective at a time, so all objectives must be combined into one function. For this purpose, an extension of this algorithm has been presented by Skoglund (2012) to solve multi-objective time-dependent routing problems using the concept of Pareto efficiency. The comparison between the methods demonstrated that the performance in terms of the minimum time route is similar. In the past three decades, growing concerns about emissions reduction and marine environment protection have also led to considering ship seakeeping performances in routing strategies, as reported in Pennino et al. (2020). This study employed the Dijkstra shortest path algorithm, constrained to maximise a non-negative cost function, namely the Seakeeping Performance Index. The results showed an increase in seakeeping performance up to 50%, without significantly affecting the voyage duration and the route length. More generally, the variability of the weather phenomena such as rogue waves and sudden storms are difficult to prevent with sufficient warning. In this respect, the master and the crew need to be supported by the on-board systems that have the capability to respond dynamically to such events. In this respect, Lindemann et al.

(1977) were the first to emphasise the importance of an onboard surveillance system in rough sea conditions, based on the requirements of the Norwegian crew. Subsequently, in the early 1990s, a new prototype of an onboard-based guidance and surveillance system was presented by Huss and Olander (1994). From 2005 to 2008, the European Committee worked on the Advanced Decision Support System for Ship Design (ADOPT) project, aiming at reducing navigational risk's through a prototype decision support system. The system was validated in a simulated navigation environment, demonstrating its potential to enhance onboard safety through predictive risk assessment and hazard identification. However, the system was not applicable in real operational conditions due to several limitations. The most critical issues were the high computational time (up to three hours for the sea state assessment) and the sensitivity of the results to the accuracy of input data and the variation of the ship loading conditions. Nowadays, these issues are still open, and it should be emphasised, that most ships still employ visual measurement methods to estimate the sea state conditions, which mainly depend on the optical perception of the observer.

Recently, with the advent of autonomous navigation, the ability to constantly assess sea state conditions using on-board sensors has become essential for adaptive navigation and real-time hazard avoidance. In this regard, in June 2019, the 101st session of the Maritime Safety Committee (MSC) approved the first interim guidelines for Maritime Autonomous Surface Ship (MASS) trials (IMO, 2019), where the importance of having on-board a proper infrastructure to provide appropriate strategies to mitigate the effects of an incident and/or failure of systems was emphasised. In this respect, a few autonomous ship prototypes have been tested, such as the *Yara Birkeland*, which was the first fully electric and autonomous container vessel with zero emissions (Evensen, 2020), or the *Suzaku*, designed by Japanese shipping companies that sails a distance of approximately 790 kilometres between Tokyo Bay and Ise Bay (Butsanets et al., 2021). These experimental tests are still too far from the idea that the ship can navigate autonomously, without a crew on-board and for long distances in fully loaded conditions. In conclusion, it is important to stress that sea state estimation is an activity that started in the past and still presents some challenges. Without solid cooperation between academia, research centres and shipping companies, achieving these goals will remain a challenge in the future.

1.3 Sea state observation methods

Over time, several technologies have been developed to measure the sea surface. As shown in Table 1.1, these methods can be distinguished in terms of spatial coverage, temporal resolution, accuracy and cost. The oldest approach involves in situ measurements using wave buoys. The buoys, either moored or drifting, are usually equipped with inertial sensors that measure their motion in response to sea surface dynamics. The analysis of the measured time series enables not only the estimation of the wave spectrum, but also contributes to the enhancement of oceanographic databases. In this respect, the first pioneering studies conducted by oceanographers, coastal engineers and geologists (Moskowitz, 1964; Michel et al., 1968; Mansard and Funke, 1991; Michel et al., 1999), focused on estimating wave spectra through the spectral analysis of buoy motions. The buoys provide sea state estimates with high spatio-temporal resolution, but the coverage is limited to the location where they are installed. Nowadays, the wave buoys are scattered along the North America and Western Europe coastal margins, with a significant gap in global coverage, especially in the Southern Ocean and along the tropics (Ardhuin et al., 2019). This spatial gap reduces the applicability of wave buoy measurements for estimating the sea state encountered by a ship along its route. Besides, the buoys are expensive to install and can be damaged by extreme weather conditions. Alternatively, remote sensing techniques, such as satellite altimeters or synthetic aperture radars, provide synoptic coverage over large ocean areas (Ardhuin et al., 2019). However, processed sea state data often become available with a delay ranging from hours to days, so making them unsuitable for real-time applications on a local scale. Another common method involves the use of wave radars, installed on board the ships. However, despite their widespread availability, wave radar systems are expensive and do not represent a cost-effective solution for shipping companies (Nielsen et al., 2019). Furthermore, they have several technical limitations, such as difficulties in accurate wave height estimation and high sensitivity to adverse weather conditions. In fact, wave radars are often used alongside ultrasonic altimeters to enhance wave height measurements. Other solutions derive from the employment of ocean data, obtained through numerical wave models, that offer an alternative solution to produce global or regional sea state condition databases. These models employ observed data and apply physical equations to forecast sea states. However, their accuracy depends on the quality of the input data and the ability of the model to resolve local dynamics. The most common numerical wave models, available to provide global and regional sea forecasts, are WAM (Komen et al., 1996), SWAN (Booij et al., 1999) and WW3 (Tolman et al., 2002). These three models are similar but differ in terms of numerical implementation and parameterisation of the physical processes. However, they require accurate input data to set the initial conditions of the model and are affected by modelling uncertainties, especially in complex atmospheric conditions. As concerns global wave hindcast data, the European Center for Medium-Range Weather Forecasts releases large quantities of atmospheric and ocean data. For instance, ocean data are hourly provided on a global scale, typically using a grid resolution of 0.25 degrees (Hersbach et al., 2020). These data provide unvaluable statistical information useful for predictive models and the reanalysis product, such as the ERA5, which is widely used as ground-truth dataset. Another possible approach relies on shipboard measurements. Ship motions and accelerations can be measured using high-precision inertial sensors or, alternatively, through low-cost measurement systems, such as standard smartphones, which are typically equipped with sensors capable of recording raw inertial data at an established sampling frequency. These measurements can be used as input to the numerical model (so-called wave buoy analogy concept model) that estimates the main wave parameters. In conclusion, the choice of the measurement method depends on various factors, such as spatio-temporal scale, availability of instrumentation and resistance to environmental variability. In the literature, two reviews about the sea state observation methods are published, reporting a detailed description of the main pros and cons of each technique (Rossi et al., 2021; Ardhuin et al., 2019).

Observation Method	**Spatial Coverage**	**Real-time**	**Cost**
Wave Buoys	Local	Yes	High
Satellite (Altimeter / SAR)	Global	No	Medium
Numerical Models	Global / Regional	Yes (forecast)	Medium
Shipboard Measurements	Local (along the ship route)	Yes	Low (onboard sensors)

Table 1.1: Comparison of sea state observation methods.

1.4 The wave buoy analogy: state of the art

In recent years, several ships have been equipped with inertial sensors to measure their responses to waves encountered during navigation. These measurements can be used as input for the numerical models that estimate the sea state conditions. The *wave buoy analogy* is the most relevant sea state estimation technique, although it has not been implemented as part of on-board decision support systems. This model is based on the linear wave theory, which mathematically relates the incident waves and the ship responses, assuming that the vessel acts as a wave buoy. In this respect, three main issues need to be considered. First, ships have more complex geometries, as regards wave buoys, that reflect into greater uncertainties in computing the relevant transfer functions. Besides, the ships are not fixed at a specific point, but they advance at a certain speed, encountering the waves at a frequency different from the absolute one, depending on the Doppler Shift effect. Finally, ships act as low-pass filters, attenuating their responses at high-frequency wave components. The first pioneering study on the employment of ship motion measurements to estimate the sea state conditions dates back to the mid-70s, when Takekuma and Takahashi (1973) employed the wave buoy analogy model to ships with no forward speed. In the following years, several attempts were carried out to take into account the Doppler shift for ships advancing at head and bow seas (Isobe et al. (1984); Kobune and Hashimoto (1986) and among others) and then, at stern and following seas (Iseki and Ohtsu, 2000). Several years later, Nielsen (2007) validated the wave buoy analogy method by comparing sea state estimates obtained from full-scale motion measurements with those from traditional wave buoys. Since then, researchers and shipping companies have increased their interest in finding a reliable method that accurately estimates sea state conditions to support and improve the on-board safety. Conceptually, the ”*ship as a buoy*” can be used in physical models formulated in the frequency or time domain, or through data-driven approaches, i.e., machine learning (ML) techniques, as depicted in Figure 1.3.

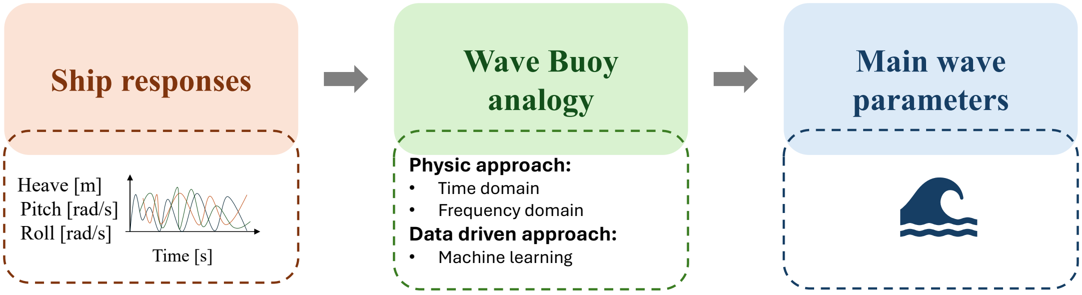

Figure 1.3: Wave buoy analogy schedule

Each method presents specific advantages and limitations. Many procedures have been developed in the frequency domain, while only a few research focuses on the time domain procedure. They are mainly based on the employment of Kalman filter, which computes sea state procedure in real time by iteratively updating the state vector at the current and next time instant. In the literature, the gap in the time-domain approach is due to the lack of studies under realistic scenarios. For instance, Nielsen et al. (2015) proposed a time domain approach that introduces a novel method to identify the wave peak period in real-time entirely from experimental data for regular waves, representing an unfeasible scenario in a real ocean environment. Other time domain attempts have been proposed by Pascoal and Soares (2009) and Pascoal et al. (2017), who estimated sea state conditions using the Kalman filter. The former study relies on the analysis of the simulated ship motions and hydrodynamic data for zero-velocity conditions, while the latter uses full-scale measured data, where a tendency to underestimate the significant wave height and overestimate the directional spread was observed. In both cases, sea state estimation is highly dependent on the availability of accurate transfer functions, which could be a principal source of errors. Numerical models in the frequency domain use spectral analysis to describe ship responses at several sea state conditions encountered by the ship along its route. The main advantage is the possibility to accurately estimate the wave spectra, if stationary conditions[1] are verified. Considering the ship's behaviour, a minimum time window of 20 to 25 minutes is generally required to obtain reliable estimates of sea state parameters, as shorter intervals can introduce excessive variability in the assessment of sea state condition while long time windows (e.g., exceeding 3 hours) may lead to non-stationary effects due to changes in sea state conditions, vessel speed or heading angles during measurements (Iseki and Nielsen, 2015; Nielsen, 2017). Frequency-domain algorithms can be classified into parametric and non-parametric methods. Parametric approaches estimate wave spectra fitting predefined spectral shapes (e.g., JONSWAP). Otherwise, non-parametric methods estimate the spectra using discretised points in the frequency-directional domain, without a priori assumptions about the spectral shape. In the early 2000s, Nielsen (2006)

[1] this assumption is not realistic for the sea, which is a dynamic environment.

compared parametric and non-parametric approaches, using container ship data, concluding that both methods can provide a reliable sea state estimation. Among the non-parametric procedures the Bayesian method is widely used and, according to Goda (2010), it shows superior performance compared to other methods, such as the extended maximum likelihood method (Isobe et al., 1984), the maximum entropy principle (Kobune & Hashimoto, 1986) and its extended version (Kim et al., 1995). Over time, several parametric methods have been developed. For instance, Hua and Palmquist (1994) provided a mathematical formulation for wave estimation at quartering and following seas, by comparing a set of parametrised theoretical heave/pitch motion spectra in the encounter frequency domain with relevant ones obtained by onboard measurements. Nielsen and Stredulinsky (2012) in this study focused only on the parametric procedure, evaluating full-scale data from small research vessels together with data from traditional wave buoys. The analysis was devoted to examining the sensitivity of sea state estimates by using sets of different vessel responses as input for the wave buoy analogy. Many years later, Piscopo et al. (2020) developed a parametric wave spectrum assessment procedure based on maximising the Pearson correlation coefficient for unimodal and bimodal long-crested sea states. This study investigated a wide range of unimodal scenarios, while only a limited number of bimodal scenarios were analysed. Inspired by Piscopo et al. (2020), a new method was proposed by Zago et al. (2023) for the parametric estimation of the waves encountered by the ship, where the main differences consist in not considering the main wave direction as known a priori and in applying the Weibull distribution function for the parametrisation of the wave spectra. From this point of view, another effort was carried out by Piscopo et al. (2024), which proposed a new algorithm for unimodal and short-crested seas using the Spearman correlation coefficient between measured and theoretical spectra, providing a reliable sea state estimation. This procedure was also validated with a full-scale ship motion dataset, measured onboard a 2,800 TEU containership. The measured sea state parameters have been compared with the relevant ones provided by the onboard wave radar and the ERA5, released by the European Centre for Medium-Range Weather Forecasts (Ascione et al., 2026). On the other hand, as concerns the bimodal seas, Nielsen (2007) proposed the partitioning technique to separately estimate the swell and wind sea spectra using a combination of Bayesian and parametric methods. A further theoretical development has been achieved by Montazeri et al. (2016), who proposed a method that formulates an optimisation problem based on the energy balance between measured and theoretical spectral moments, including a sequential partitioning algorithm to separately detect the swell and wind sea components. Recently, Piscopo et al. (2025) proposed a new procedure for bimodal sea states, in which the ship accelerations, due to wind sea and swell components, are preliminarily estimated by iteratively applying high pass filters to the ship motion time history. The results of this procedure show a reliable estimation of the significant wave height and the wave peak period, once an external source, such as the ERA5 reanalysis service, provides the wave prevailing direction. Instead, the data-driven approaches do not require the knowledge of ship transfer functions, thereby avoiding the uncertainties typically associated with them, which are strongly dependent on the vessel speed and loading conditions. Moreover, it has been demonstrated that the spectro-temporal analysis of ship motions, using the data-driven approach, does not require long ship motion time series (Tu et al., 2018; Majidiyan et al., 2024). However, these approaches rely on extensive and often redundant datasets to ensure a reliable training phase. In recent years, several studies have investigated the reliability of different data-driven techniques. For instance, Nielsen et al. (2024) applied both the gradient boosting framework LightGBM and the Artificial Neural Network (ANN) to a large dataset of ship motions, estimating sea state conditions with high accuracy. Further effort was made in Kawai et al. (2021), where Convolutional Neural Networks (CNNs) were tested. Both studies demonstrate the high reliability of machine learning techniques, inspiring their use in future research. As years went by, the knowledge about the wave buoy analogy reached a sufficient level of reliability, even if new approaches are being explored. For instance, to provide a more reliable sea state estimation, Mittendorf et al. (2022) also tested the combination of physics-based and machine learning-based approaches, which notably improved the sea state estimation results. Alternatively, Nielsen et al. (2019) proposed using the ship as part of a cooperative data network, while Mounet (2023) explored the possibility of estimating sea state conditions based on measurements from multiple observation platforms. In this respect, it should be emphasized that one of the main strengths of the wave buoy analogy is the possibility of using not only the ships responses but also integrating them with measurements provided by other surface floating structures. In this respect, the wave buoy analogy limits and advantages were highlighted by Nielsen (2017), Majidian et al. (2022) and Nielsen et al. (2023), who provide extensive literature reviews. As this technique represents a principal model to estimate the sea state conditions, two numerical procedures were developed in this thesis, based on the wave buoy analogy assumptions.

1.5 Scope and Novelty of the present thesis

This PhD thesis addresses the sea state estimation challenge by pursuing two main objectives:

$\mathbf{O}_1$: Develop a code that simulates ship motions in the time-domain to generate simulated dataset.

$\mathbf{O}_2$: Develop new unimodal and bimodal short-crested sea state estimation models, based on a frequency-domain approach.

To achieve these objectives, three MATLAB codes were developed. The code related to Objective 1 solves the Cummins equations in the time domain, generating a comprehensive dataset of synthetic ship motions. As concerns the Objective 2, two novel parametric procedures were developed in the frequency domain. The first procedure focuses on unimodal short-crested sea state condition, while the second is designed to estimate bimodal sea state conditions obtained by the superposition of wind sea and swell components. Therefore, the novelty of these procedures lies in:

- Employment of rank correlation coefficients to compute the correlation between measured and theoretical wave spectra (Piscopo et al., 2024).
- Separately determine the ship accelerations, due to wind sea and swell components, by iteratively applying high pass filters to the ship motion time histories. (Piscopo et al., 2025).

Chapter 2

Ocean Waves

This Chapter provides an overview of ocean wave theory and the basic theoretical concepts required to describe the sea state conditions.

2.1 Irregular wave modelling

Waves are generated by large-scale and long-duration atmospheric phenomena. The wind that blows on the sea surface generates a local storm, which produces wind waves. As the wind speed increases, the fetch[2] and the severity of the waves also grow. Once the wind waves move out of the storm area, they gradually become more regular and smoother, transforming into swell waves. In general, wind waves can travel long distances across the globe in the absence of obstacles, while swell can reach distant sea areas, where other storms develop new wave systems. This allows interaction among local wind seas and swell. The sea state is classified as *unimodal* if it is dominated by a single wave system (either wind sea or swell). Alternatively, if the coexistence of two distinct wave systems occurs, it is classified as *bimodal*. Over time, the wave systems spread sideways and interact with waves coming from different directions, generating *short-crested* sea state conditions, which are the most commons ones.

When observing an irregular wave with respect to the mean sea level (MSL), the main wave parameters, shown in Figure 2.1, are the following ones:

- wave amplitude (η): it is the vertical distance from the mean sea level to the wave crest or trough.
- wavelength (λ): it is the horizontal distance between two successive crests or troughs.
- wave height (H): it is the vertical distance between a crest and its adjacent trough.

[2]Fetch is the horizontal distance over which the wind blows with a relatively constant speed and direction over a body of water.

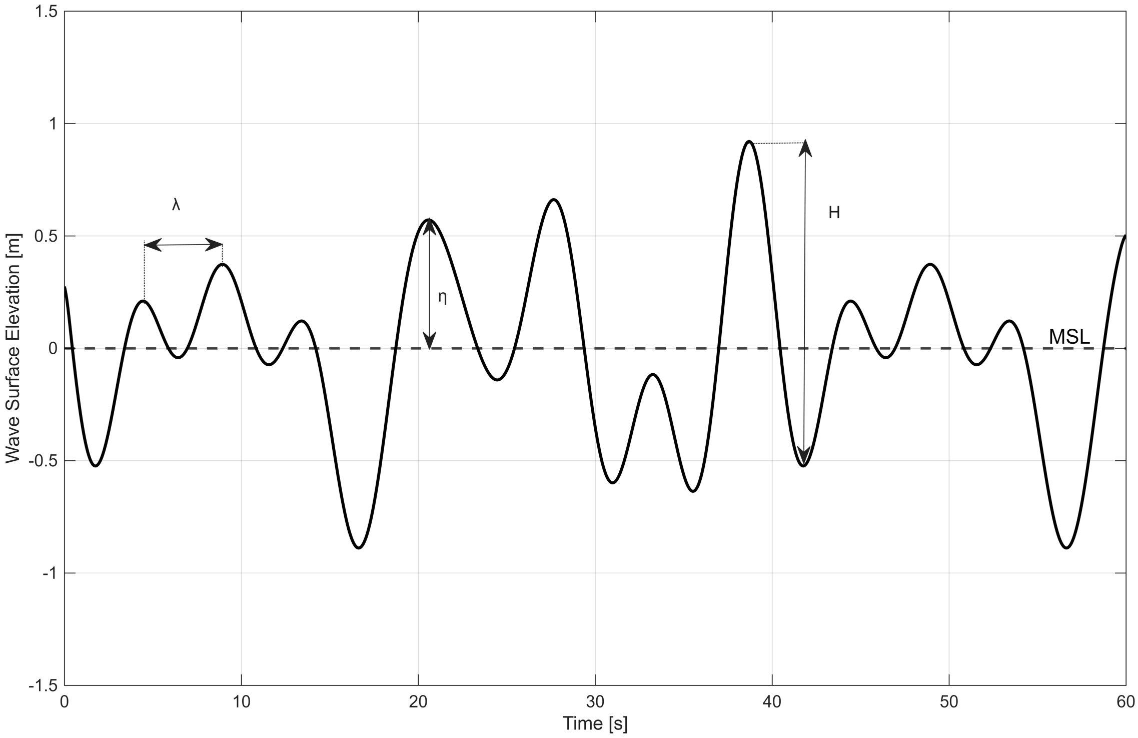

Figure 2.1: Representation of an irregular wave relative to the mean sea level (MSL).

Denoting by N the total number of observations of the i-th wave amplitude η_i, the following statistical parameters can be introduced:

- mean sea surface level ($\overline{\eta}$):

$$\mathbb{E}[\eta] = \overline{\eta} = \frac{1}{N}\sum_{i=1}^{N}\eta_i \tag{2.1}$$

- wave variance (σ^2) relative to mean sea level:

$$\sigma^2 = \frac{1}{N}\sum_{i=1}^{N}(\eta_i - \overline{\eta})^2 \tag{2.2}$$

  Assuming that η_i represents a stationary process with mean $\mathbb{E}[\eta]$, the variance is defined as $\sigma^2 = \mathbb{E}[(\eta - \mathbb{E}[\eta])^2]$. If the process is zero-mean (i.e., $\mathbb{E}[\eta] = 0$), this simplifies to $\sigma^2 = \mathbb{E}[\eta^2]$.

- standard deviation (σ) relative to mean sea level:

$$\sigma = \sqrt{\sigma^2} \tag{2.3}$$

According to the linear wave theory (Airy, 1845), the irregular sea surface can be described as a linear superposition of many regular sinusoidal components, each one with independent amplitudes and phases (Lewis et al., 1988). The sea surface elevation $\eta(x, y, t)$, relative to the mean sea level, observed at a fixed location x, y at a given time t, can be modelled as follows:

$$\eta(x, y, t) = \sum_n a_n \cos\left[k_n(x \cos\mu_n + y \sin\mu_n) - \omega_n t + \phi_n\right] \tag{2.4}$$

For the n-th wave component, a_n denotes the amplitude, ϕ_n is the random phase angle uniformly distributed in the interval $[0, 2\pi]$, ω_n is the angular frequency, μ_n is the wave propagation direction and $k_n = \frac{2\pi}{\lambda_n}$ is the wave number, with λ_n denoting the wavelength.
The angular frequency ω_n and the wave number k_n of the n-th wave component are related by the linear dispersion relation:

$$\omega_n^2 = g k_n \tanh(k_n d) \tag{2.5}$$

where g is the gravitational acceleration and d is the water depth. In deep water conditions ($d > \lambda_n$), $\tanh(k_n d) \approx 1$ so as the Equation 2.5 simplifies to $\omega_n^2 = g k_n$. Otherwise, if the water depth is much less than the wavelength ($d < \lambda_n$) so as $\tanh(k_n d) < 1$, the dispersion relation is equal to $\omega_n^2 = g k_n^2 d$.

2.2 Wave Spectra

Since the components in Equation 2.4 have random phases, the total variance σ^2 of the sea surface elevation η corresponds to the sum of the variances of the individual sinusoidal components:

$$\sigma^2 = \sum_n \sigma_n^2 = \sum_n \frac{a_n^2}{2} \tag{2.6}$$

In order to describe how this variance is distributed in the frequency domain, the *wave variance spectrum* $S_\sigma(\omega)$ is introduced. This function represents the spectral density of the variance with respect to the angular frequency ω. It can be formally defined as the limit of the variance per unit frequency interval as the interval width tends to zero. Denoting by $\delta\sigma$ the variance of each wave component corresponding to a narrow frequency band of width $\delta\omega$ centred at ω, the *wave variance spectrum* can be defined by Equation 2.7:

$$S_\sigma(\omega) = \lim_{\delta\omega \to 0} \frac{\delta\sigma}{\delta\omega} \tag{2.7}$$

Integrating $S_\sigma(\omega)$ over all frequencies, the variance σ of the wave system is expressed as follows:

$$\sigma^2 = \int_0^\infty S_\sigma(\omega)\, d\omega \tag{2.8}$$

Since the wave energy per unit area E is proportional to the variance, a direct relationship between the wave spectrum and the wave energy can be established:

$$E = \rho g \sigma^2 = \rho g \int_0^{\infty} S_{\sigma}(\omega)\, d\omega \tag{2.9}$$

where ρ is the water density.

To account for the directional distribution of wave energy, the *directional wave spectrum* $S(\omega, \mu)$ is introduced by Equation 2.10:

$$S(\omega, \mu) = \lim_{\delta\omega, \delta\mu \to 0} \frac{\delta\sigma}{\delta\omega, \delta\mu} \tag{2.10}$$

This two-dimensional spectrum $S(\omega_n, \mu)$ describes how the variance of the waves is spread over both the wave frequency ω and wave direction μ. Therefore, the total variance is defined by integrating over all directions and frequencies as reported in Equation 2.11:

$$\sigma^2 = \int_0^{2\pi} \int_0^{\infty} S(\omega, \mu) d\omega d\mu \tag{2.11}$$

2.3 Spectral moments and Sea state parameters

The spectral moments m_n are calculated as the integral of the n-th power of frequency ω^n multiplied by the wave spectrum $S(\omega)$, as follows:

$$m_n = \int_0^{\infty} \omega^n S(\omega) d\omega \tag{2.12}$$

where $n \in \{-1, 0, 1, 2, 3, 4\}$ indicates the relevant order.

The most common wave parameters used to describe the sea state conditions are the significant wave height H_s, the wave peak period T_p and the prevailing mean wave direction μ_m.

The significant wave height H_s, is defined as the average of the highest 1/3 of the waves heights and it is estimated as follows:

$$H_s = 4\sqrt{m_0} \tag{2.13}$$

The wave peak period T_p corresponds to the time interval between two successive peaks (crests or troughs). In case of irregular sea state conditions it corresponds to the wave peak frequency ω_p, according to the following equation:

$$T_p = 2\pi / \omega_p \tag{2.14}$$

where $\omega_p = \text{argmax}_\omega[S(\omega)]$.
The prevailing main wave direction μ_m represents the average direction from which the prevailing wave energy comes:

$$\mu_m = \arctan\left(\frac{\int_0^{2\pi}\int_0^{\infty} \sin\mu\, S(\omega,\mu)\, d\omega d\mu}{\int_0^{2\pi}\int_0^{\infty} \cos\mu\, S(\omega,\mu)\, d\omega d\mu}\right) \tag{2.15}$$

2.4 Theoretical wave spectra

The theoretical wave spectra are used as a model of representation of the wave energy distribution to describe the spectral characteristics of irregular waves. The theoretical spectrum, most commonly employed to describe the state of the sea in terms of an energy spectrum, is the two-parameter Bretschneider (1959) spectrum. The main assumptions of this model are the following ones: sea state conditions are fully developed, the water depth and fetch are infinite, swell and current are negligible. It is defined according to Equation 2.16:

$$S_B(\omega) = \frac{A}{\omega^5}\exp\left(-\frac{B}{\omega^4}\right) \tag{2.16}$$

where $S_B(\omega)$ is the spectral energy density, ω is the angular frequency, while A and B are empirical constants that depend on the significant wave height H_s and the mean wave period T_1 as follows:

$$A = 173 \cdot \frac{H_s^2}{T_1^4} \tag{2.17}$$

$$B = \frac{691}{T_1^4} \tag{2.18}$$

where $T_1 = 2\pi\frac{m_0}{m_1}$ and $H_s = 4\sqrt{m_0}$.
This model is particularly suited for fully developed seas, as well as for seas during formation or extinction phases. For this reason, it is widely adopted in the fields of naval architecture and offshore engineering. Starting from this theoretical spectrum, other models have been presented in literature, namely the Pierzon-Moskowitz, the ISSC and the ITTC spectra among others (Pawlowski, 2011). They are formally identical, but differ only with respect to the parameters used as input to determine the A and B parameters, as reported in Stansberg et al. (2002) and shown in Table 2.1.

2.4.1 Pierzon Moskowitz spectrum

The one-parameter Pierson-Moskowitz spectrum was introduced in 1964, using as input the wind speed V measured at 19.5 meters above the sea surface (Moskowitz, 1964), according to Equation 2.19:

Spectrum	A and B defined in terms of	Sea State Applicability
Bretschneider	Significant wave height and mean period	Fully developed, rising and falling seas.
One-parameter Pierson-Moskowitz	Significant wave height and peak period	Fully developed sea
ISSC	Significant wave height and mean period	Fully developed sea
ITTC	Significant wave height and one of: energy period, peak period, mean period, or zero-crossing period	Fully developed sea

Table 2.1: Overview of the theoretical wave spectra.

$$S_{PM}(\omega) = \frac{\alpha g^2}{\omega^5} \exp\left[-\beta \left(\frac{g/V_{19.5}}{\omega}\right)^4\right] \tag{2.19}$$

where α and β are equal to 8.10×10^{-3} and 0.74 respectively.
This spectrum model was developed from the analysis of the wave records measured in the North Atlantic by both British and American marine weather stations. From 460 available point spectra, Moskowitz (1964) selected a sample of 54 spectra that were grouped and re-distributed according to five wind speed values, namely 20, 25, 30, 35 and 40 knots. In this respect, in Figure 2.2, the Pierzon Moskowitz spectrum corresponding to different wind speeds is shown. The Pierson-Moskowitz spectrum can also be expressed as a function of the significant wave height H_s and the wave peak period T_p as reported in DNV (2010) according to Equation 2.20:

$$S_{PM}(H_s, T_p, \omega) = \frac{5}{16} H_s^2\, \omega_p^4\, \omega^{-5} \exp\left(-\frac{5}{4}\left(\frac{\omega_p}{\omega}\right)^4\right) \tag{2.20}$$

where $\omega_p = \frac{2\pi}{T_p}$ is the peak circular frequency.

2.4.2 JONSWAP spectrum

In order to account for sea state conditions with higher waves and frequency shifts that occur in fetch-limited conditions (typical of the North Seas), the JONSWAP spectrum was introduced in the early 70s by Hasselmann et al. (1980). It is mathematically expressed according to Equation 2.21(DNV, 2010):

$$S_J(H_s, T_p, \gamma, \omega) = A_\gamma\, S_{PM}(H_s, T_p, \omega)\, \gamma^{\exp\left(-0.5\left(\frac{\omega-\omega_p}{\hat{\sigma}\omega_p}\right)^2\right)} \tag{2.21}$$

where S_{PM} is the Pierzon Moskowitz spectrum provided by Equation 2.20, $A_\gamma = 1 - 0.287\ln(\gamma)$ is a normalising factor, γ denotes the spectral width parameter and $\hat{\sigma}$ is the spectral

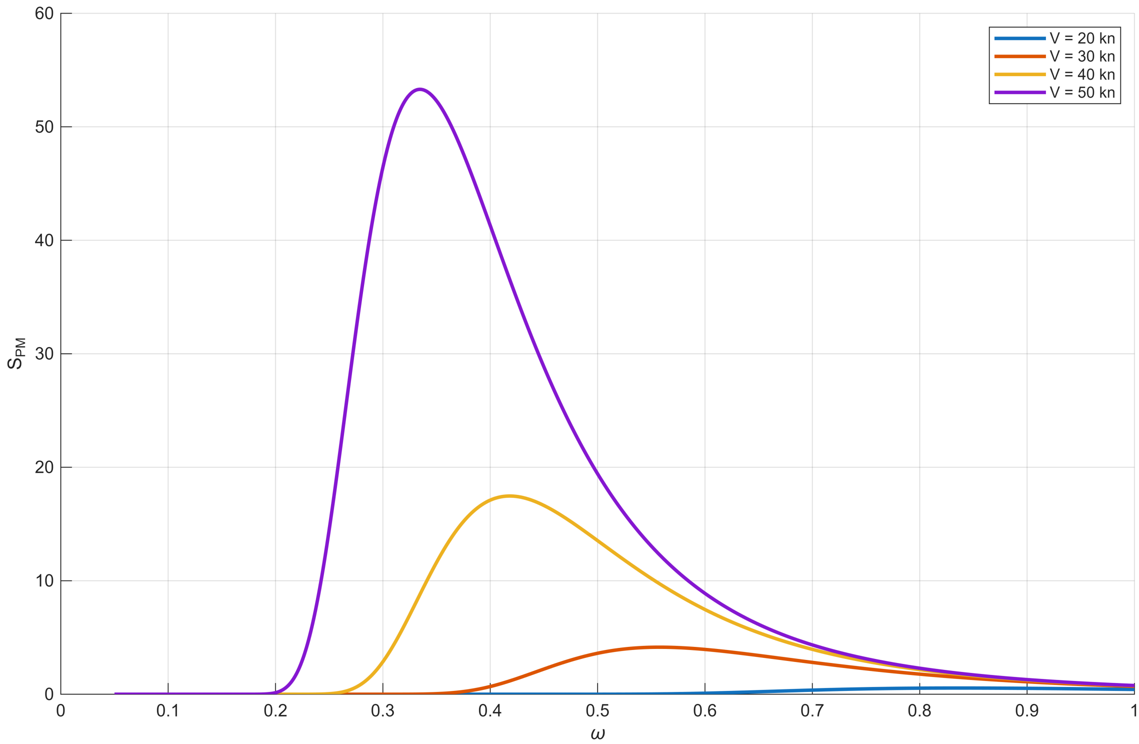

Figure 2.2: Pierzon Moskowitz spectra for different wind speeds according toMoskowitz (1964)

width parameter that depends on the peak circular frequency as reported below:

$$\hat{\sigma} = \begin{cases} 0.07 & \text{for } \omega \leq \omega_p \\ 0.09 & \text{for } \omega > \omega_p \end{cases} \tag{2.22}$$

The JONSWAP spectrum resembles the Pierson-Moskowitz spectrum when $\gamma = 1$.

2.4.3 TMA spectrum

The TMA spectrum was developed for non-breaking waves in finite water depth. It is expressed as a modified JONSWAP spectrum; indeed, it is obtained by multiplying the JONSWAP spectrum by a limited depth function as expressed by Equation 2.23:

$$S_{TMA}(\omega) = S_J(H_s, T_p, \gamma, \omega)\phi(\omega, d) \tag{2.23}$$

The depth function $\phi(\omega, d)$ is given by Equation 2.24:

$$\phi(\omega, d) = \frac{\omega^5 \frac{dk}{d\omega}}{2g^2k^3} \tag{2.24}$$

By the dispersion relation provided by Equation 2.5 the depth function can be rewritten as follows:

$$\phi(\omega, d) = \frac{cosh^2(kd)}{sinh^2(kd) + \frac{\omega^2 d}{g}} \tag{2.25}$$

2.4.4 The Ochi-Hubble wave spectrum

The spectral models employed for modelling the bimodal sea state conditions are generally obtained as the sum of both the wind $S_w(\omega)$ and swell $S_s(\omega)$ components, as follows:

$$S_b(\omega) = S_w(\omega) + S_s(\omega) \tag{2.26}$$

The Ochi-Hubble wave spectra model is designed to describe waves characterised by the presence of wind (high-frequency part) and swell (low-frequency part[3]) components, as a combination of two Gamma probability distributions as reported in Equation 2.27:

$$S_{OH}(\omega) = \frac{1}{4}\sum_{j=1}^{2}\left[\frac{\left(\frac{4\tilde{\lambda}_j+1}{4}\omega_{pj}^4\right)^{\tilde{\lambda}_j}}{\Gamma(\tilde{\lambda}_j)}\frac{H_{sj}^2}{\omega^{4\tilde{\lambda}_j+1}}\exp\left(-\left(\frac{4\tilde{\lambda}_j+1}{4}\right)\left(\frac{\omega_{pj}}{\omega}\right)^4\right)\right] \tag{2.27}$$

where $j = 1, 2$ corresponds to the lower and higher frequency parts, H_{sj} is the significant wave height, λ_j is the shape parameter and Γ is the gamma function. This spectrum is commonly used in the offshore standards for structural design (DNV, 2000).

[3]The swell spectrum has a narrow frequency band, and the swell peak is usually to the left of the wind waves.

Chapter 3

Time-domain ship motion simulations

This Chapter describes the MATLAB code developed to generate a comprehensive dataset of simulated ship motion time series by solving the Cummins equations for heave, pitch and roll motions. The ship motions dataset will be employed as input for the subsequent validation phase of the sea state assessment procedures. The following paragraphs provide further details.

3.1 Foundations of the code

The code allows accounting for short-crested seas characterised by the coexistence of multiple wave systems with different propagation directions. In such conditions, the energy spectrum of the waves at a fixed point in the ocean contains contributions from waves coming from different directions that differ from the predominant ones. The short-crested wave energy spectrum in the absolute frequency domain is computed as the product between the wave spectrum for long-crested sea state conditions $S(\omega)$ and a directional spreading function $D(\theta)$, according to Equation 3.1:

$$S(\omega,\theta) = S(\omega)D(\theta) \tag{3.1}$$

The directional spreading function, in turn, is given by Equation 3.2:

$$D(\theta) = \frac{\Gamma\left(1+\frac{n}{2}\right)}{\sqrt{\pi}\,\Gamma\left(\frac{1}{2}+\frac{n}{2}\right)}\cos^n(\theta), \quad -\frac{\pi}{2} \le \theta \le \frac{\pi}{2} \tag{3.2}$$

where n denotes the spreading parameter and θ is the angle between the elementary wave train and the prevailing wave direction.
The mathematical relationship between the encounter ω_e and the absolute ω wave frequencies depends on the ship speed U and the heading angle μ of the elementary wave train as regards the ship reference frame. In Figure 3.1, the direction from which the waves originate (come from) is defined by the angle β relative to the North, while the ship bow orientation is defined

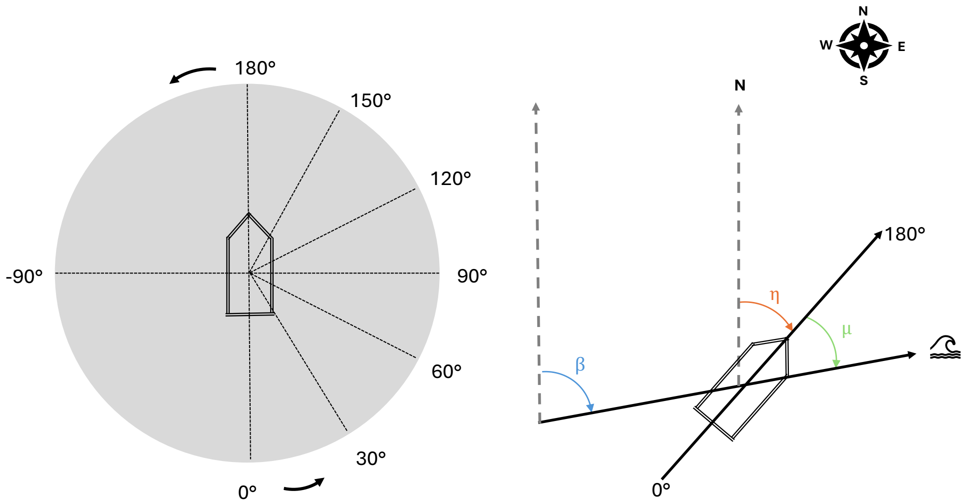

Figure 3.1: Definition of the heading angle.

by the angle η with the North. However, the heading angle is computed according to Equation 3.3:

$$\mu = \beta - \eta. \tag{3.3}$$

The transformation from the absolute to the encounter wave frequency domain is given by Equation 3.4:

$$\omega_e = |\omega - \omega^2 \psi| \tag{3.4}$$

where ψ is equal to $\frac{U}{g} \cos \mu$.

It should be noted that, when transforming from the absolute to the encounter frequency domain, three distinct cases can be identified:

(a) $\mu > 90°$ ($\cos \mu < 0 \Rightarrow \psi < 0$): the relationship between the absolute and the encounter wave frequencies is bijective, so as the wave spectrum in the encounter wave frequency domain $S(\omega_e, \mu)$ is determined according to Equation 3.5:

$$S(\omega_e, \mu) = \frac{S(\omega)}{\sqrt{1 - 4\psi\,\omega_e}}. \tag{3.5}$$

(b) $\mu = 90°$ ($\cos \mu = 0 \Rightarrow \psi = 0$): no Doppler shift occurs, so as the wave spectrum in the encounter wave frequency domain $S(\omega_e, \mu)$ is given by Equation 3.6:

$$\omega_e = \omega, \qquad S(\omega_e, \mu) = S(\omega). \tag{3.6}$$

(c) $\mu < 90°$ ($\cos \mu > 0 \Rightarrow \psi > 0$): the relationship between the absolute and the encounter wave frequencies is bijective for $\omega_e \geq \frac{1}{4\psi}$ and triple-valued for $\omega_e < \frac{1}{4\psi}$. In the latter case, three absolute wave frequencies correspond to the same encounter one, as shown in Figure 3.2, so as the wave spectrum in the encounter frequency domain $S(\omega_e, \mu)$ is computed as the sum of three distinct contributions according to Equation 3.7:

$$S(\omega_e, \mu) = \left[\frac{S(\omega_1, \mu) + S(\omega_2, \mu)}{\sqrt{1 - 4\psi\omega_e}} + \frac{S(\omega_3, \mu)}{\sqrt{1 - 4\psi\omega_e}} \right] \tag{3.7}$$

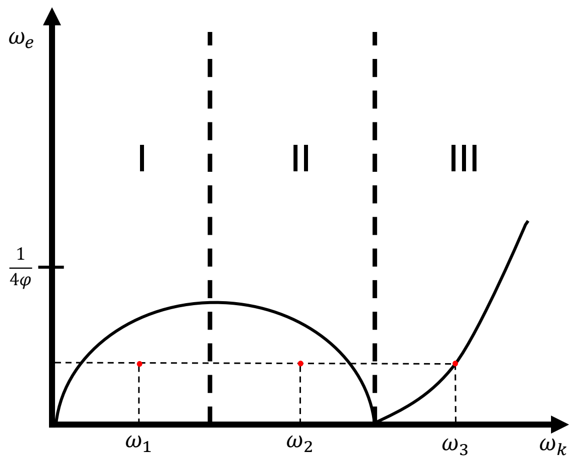

Figure 3.2: Triple-valued function problem between absolute and encounter wave frequencies.

3.2 Time-domain motion equations

The time histories of coupled heave/pitch and roll motions are generated by a dedicated code, based on the Cummins (1962) equations, according to Equation 3.8:

$$\begin{cases} (\Delta + A_{33}^{\infty})\ddot{\xi}_3 + B_{33}^{\infty}\dot{\xi}_3 + \int_{-\infty}^{t} k_{33}(t-\tau)\dot{\xi}_3(\tau)\,d\tau + C_{33}\xi_3 + \\ \quad + A_{35}^{\infty}\ddot{\xi}_5 + B_{35}^{\infty}\dot{\xi}_5 + \int_{-\infty}^{t} k_{35}(t-\tau)\dot{\xi}_5(\tau)\,d\tau + C_{35}\xi_5 = F_3(\mu, t) \\ A_{53}^{\infty}\ddot{\xi}_3 + B_{53}^{\infty}\dot{\xi}_3 + \int_{-\infty}^{t} k_{53}(t-\tau)\dot{\xi}_3(\tau)\,d\tau + C_{53}\xi_3 + \\ \quad + (I_{55} + A_{55}^{\infty})\ddot{\xi}_5 + B_{55}^{\infty}\dot{\xi}_5 + \int_{-\infty}^{t} k_{55}(t-\tau)\dot{\xi}_5(\tau)\,d\tau + C_{55}\xi_5 = F_5(\mu, t) \\ (\Delta + A_{44}^{\infty})\ddot{\xi}_4 + B_{44}^{\infty}\dot{\xi}_4 + \int_{-\infty}^{t} k_{44}(t-\tau)\dot{\xi}_4(\tau)\,d\tau + C_{44}\xi_4 = F_4(\mu, t) \end{cases} \tag{3.8}$$

having denoted by A_{ij} the added mass, B_{ij} the radiation damping and C_{ij} the combined hydrostatic and hydrodynamic restoring coefficient for the $i, j-th$ motion mode and by k_{ij} the relevant impulse response function to be determined by Equation 3.9:

$$k_{ij}(t) = \frac{2}{\pi}\int_0^{\infty} [B_{ij}(\omega_e) - B_{ij}^{\infty}]d\omega_e \tag{3.9}$$

The hydrodynamic coefficients (e.g., zero-speed added masses, radiation dampings and exciting forces) are computed using the open-source code NEMOH v2.0. The code was developed at the École centrale de Nantes and it allows determining the ship first-order hydrodynamic forces based on the boundary element method (BEM), under the assumptions of an inviscid fluid and incompressible and irrotational flow (Babarit & Delhommeau, 2015). After calculating the zero-speed hydrodynamic properties, the relevant coefficients are corrected for the forward speed effect, based on the formulation provided by Salvesen et al. (1970), as detailed in Chapter 4.

The random wave force components for short-crested sea state conditions is computed as the superposition of forces at the effective heading angle $\mu + \theta$ according to Equation 3.10:

$$F_i(\mu, t) = \int_{-\frac{\pi}{2}}^{\frac{\pi}{2}} f_i(\mu + \theta, t)d\theta \tag{3.10}$$

where μ denotes the heading angle of the prevailing wave direction and θ is the angle between the elementary wave train and the prevailing wave one.

The term $f_i(\mu + \theta, t)$ denotes the time-dependent wave force component at the heading angle $\mu + \theta$ that, in turn, is determined according to the wave spectrum transformation outlined in Subsection 3.1.

If the relationship between the absolute and the encounter wave frequencies is bijective, $f_i(\mu + \theta, t)$ is given by Equation 3.11:

$$f_i(\mu + \theta, t) = \sum_{\omega_e} \sqrt{2S_e(\omega_e)D(\theta, n)\Delta\omega_e} |\Phi_i(\mu + \theta, \omega)| cos[\omega_e t + \epsilon_i(\omega) + \varphi] \tag{3.11}$$

having denoted by Φ_i the complex wave exciting force function per unit wave amplitude of the $i-th$ motion mode, $\epsilon_i(\omega)$ the phase angle at the wave frequency ω and ϕ the random phase shift.

Otherwise, if the 3-to-1 multivalued problem between the absolute and encounter wave frequencies occurs, the random wave force at the heading angle $\mu + \theta$ is assessed by Equation 3.12:

$$f_i(\mu + \theta, t) = \sum_{\omega_e}\sum_{q=1}^{3} \sqrt{2S_e^q(\omega_e)D(\theta, n)\Delta\omega_e} |\Phi_i(\mu + \theta, \omega)| cos[\omega_e t + \epsilon_i(\omega_q) + \varphi] \tag{3.12}$$

where S_e^q is determined according to Equations 3.7.

3.3 The flow chart of the code structure

The numerical code has been developed to simulate both unimodal and bimodal short-crested sea states, adapting the procedure according to the type of dataset to be generated. The flow chart in Figure 3.3 illustrates the main steps of the simulation framework. The procedure can be summarised as follows:

- Step I: the S175 containership and hydrodynamic data are used as input.
- Step II: the short-crested wind and swell spectra are defined by selecting the significant wave height, the wave peak period, the heading angle of prevailing wave direction, the spectral width parameter, and the peak enhancement factor of both correspondent to account for unimodal (wind or swell only) or bimodal (wind + swell) sea state conditions.
- Step III: a random sea surface elevation is generated from the wind and swell spectra.
- Step IV: the corresponding random wave forces acting on the ship (heave force, pitch and roll moments) are computed and used as input for the equations of motion.
- Step V: time-domain simulations of heave, pitch and roll motions are carried out by solving the Cummins equations.

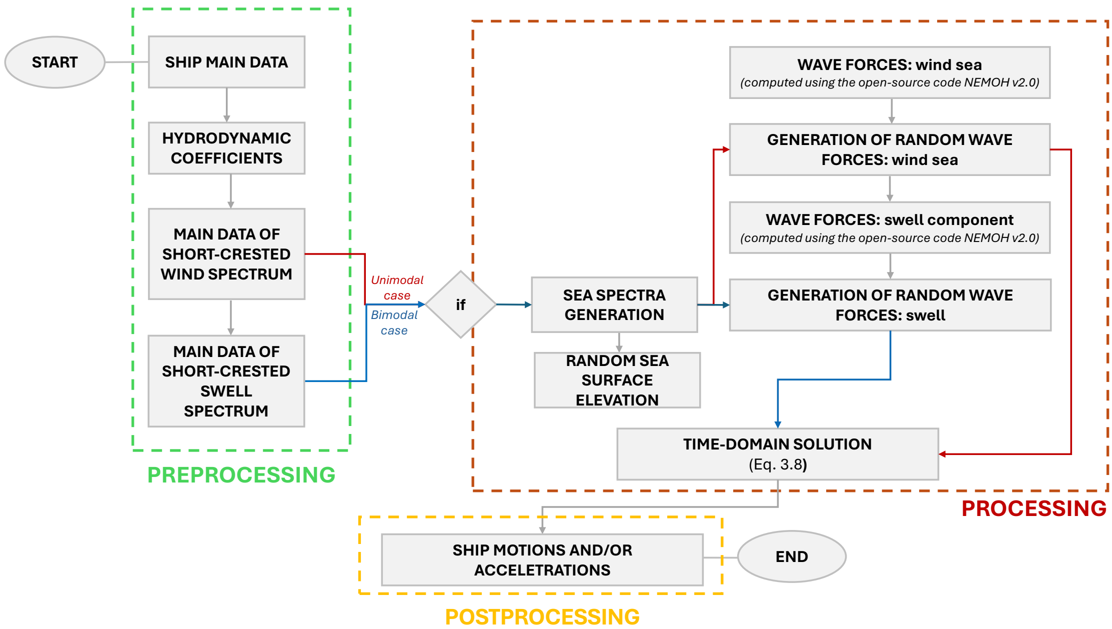

Figure 3.3: Flow chart of the simulation framework.

For each time series, the heading angle and the simulation length were systematically varied according to the dataset requirements, as further detailed in the following. Furthermore, the pseudo-code in Algorithm 1 outlines the logical sequence of the code and describes the main computational steps required to generate a compressive dataset of simulated ship motion time series.

Algorithm 1 Time–domain simulation of ship motions

Preprocessing
Load ship main data $\{v_{\text{ship}}, A_{wl}, \Delta, LCF, L_{pp}, B, GMT, BML\}$
Load hydrodynamic coefficients $\{A_{ij}(\omega), B_{ij}(\omega)\}$
Define wind sea and swell spectral parameters
Define time domain $t \in [0, T]$ and frequency domain ω
Processing
if Spectra = unimodal **then**
    $S(\omega) = S_w(\omega)$
else if Spectra = bimodal **then**
    $S(\omega) = S_w(\omega) + S_s(\omega)$
end if
Generate random sea elevation $\eta(t) = \text{RandomWave}(\omega_e, \Delta\omega, S(\omega_e), H_s, t, \text{depth})$
Load wave exciting forces per unit amplitude
Generate random wave forces
Solve coupled heave/pitch and roll Cummins equations (Equations 3.8)
$[T, Y] = \texttt{ode45}(\texttt{Cummins}_{heave,pitch})$
$[T, Y_{\text{roll}}] = \texttt{ode45}(\texttt{Cummins}_{roll})$
Postprocessing
Compute the time series of heave, pitch and roll motions
$\{z, \phi, \theta\} = \text{ship\_motion}(Y, Y_{\text{roll}}, \text{sfr})$